



# Enhancing the geometric tolerance of aluminium hybrid metal matrix composite using EDM process

T. S. Senthilkumar<sup>1</sup> · R. Muralikannan<sup>2</sup>

Received: 19 May 2018 / Accepted: 21 December 2018 / Published online: 2 January 2019  
© The Brazilian Society of Mechanical Sciences and Engineering 2019

## Abstract

A generous development of electrical discharge machining method has been stimulated in the province of metal matrix composites materials. In this extant work, the optimal condition for various output responses specifically circularity, cylindricity, perpendicularity and radial over cut are exposed by employing grey relational analysis procedure by optimizing the input process parameters alike pulse on time ( $T_{on}$ ), peak current ( $I$ ) and gap voltage ( $V$ ). The Hybrid Metal Matrix Composite material is evolved by handling the stir casting approach and then machined by exploring the input parameters using  $L_{27}$  orthogonal array. From the consequences of grey relational grade, a response table was discovered to elect the optimal conditions of the individual parameter. The most contributing input parameter is current with **69.08%**, which is determined from the ANOVA table. Finally, the optimal conditions which were acquired from the response table are peak current of 12 A, pulse on time of 50  $\mu$ s and gap voltage of 30 V and also verified through an authentication test which illustrated that optimal process parameters are competently improved by 0.1452 when compared to the predicted parameter. The machined surface is analysed using a scanning electron microscope. The results palpated that the peak current increases the number of microvoids and size of the crater was increased and the poor surface finish was achieved.

**Keywords** EDM · MMCs · Circularity (CR) · Cylindricity (CY) · Perpendicularity (PP) grey relational analysis · Pulse on time ( $T_{on}$ ) · Peak current ( $I$ ) · Gap voltage ( $V$ ) and ANOVA

## Abbreviations

EDM	Electrical discharge machining	Ton	Pulse on time
MMCs	Metal matrix composites	V	Gap voltage
HMMCs	Hybrid metal matrix composites	BN	Boron nitride
AMMCs	Aluminium metal matrix composites	TiCL	Titanium carbide
AHMMCs	Hybrid aluminium metal matrix composites	h-BN	Hexagonal boron nitride
SEM	Scanning electron microscope	Al alloy	Aluminium alloy
CR	Circularity	CNC	Computer numerical control
CY	Cylindricity	CMM	Coordinate measuring machining
PP	Perpendicularity	GRA	Grey relational analysis
ROC	Radial overcut	GRC	Grey relational coefficient
I	Peak current	GRG	Grey relational grade
		ANOVA	Analysis of variance
		S/N ratio	Signal-to-noise ratio

Technical Editor: Márcio Bacci da Silva.

✉ T. S. Senthilkumar  
senthilk.kumar6@gmail.com

<sup>1</sup> Department of Mechanical Engineering, Sree Sowdambika College of Engineering, Aruppukottai, Tamil Nadu 626134, India

<sup>2</sup> Department of Mechanical Engineering, Sethu Institute of Technology, Kariapatti, Tamil Nadu 626115, India

## 1 Introduction

Metal matrix composites (MMCs) are emerging prosperity in numerous areas including automotive, power electronics, sporting goods, aerospace and marine productions because of their excessive strength to low weight ratio, augmented mechanical and thermal properties [1]. Ordinarily, there are

several categorizations of MMCs, namely particulate-reinforced MMCs, continuous fibre-reinforced MMCs, whisker-reinforced MMCs and laminated MMCs [2]. Among these, particulate-reinforced MMCs were utilized in most important applications in the automotive sector as driveshaft, cylinder liner, engine block, connecting rods, disc brakes, etc., because of its modest cost, enhanced modulus and strength, enriched wear resistance [3]. As well as the aluminium-based MMCs are preferable for its lower density, excellent strength, toughness and corrosion resistance. The accumulation of ceramic particles is easy in the handling of aluminium metal matrix composites (AMMCs) [4]. Moreover, the mechanical and thermal properties of AMMCs are augmented with the accumulation of particulate reinforcement such as  $B_4C$ , SiC, TiC,  $Al_2O_3$ ,  $Si_3N_4$  and  $ZrB_2$  and, furthermore, by accretion of secondary particulate reinforcement such as  $Al_2O_3$ , graphite and BN. The tribological properties of AMMCs were distended [5]. By addition of more than one particulate reinforcement in AMMCs is known as aluminium hybrid metal matrix composites (AHMMCs). Plentiful techniques were accessible for generating the AHMMCs. Among those methods, stir casting process is the most uncomplicated method concerned in the formation of particulate-reinforced AHMMCs. However, it has greater dissemination of reinforced particles in the matrix medium and also it has admirable moistening properties [6].

Due to the abrasive feature of the particulate-reinforced AHMMCs, there is a difficulty in the conventional machining process which worsens the surface of the work piece and the electrode. Degradation of the tool wear rate was the decisive problem that restricts the handling of conventional machining of MMCs [7]. Therefore, the prominence has been given by the unconventional machining technique for machining AHMMCs. Regarding unconventional machining processes, there are numerous types of machining the particulate AHMMCs [8]. Among those, electrical discharge machining (EDM) arrangement was appropriate for the machining of particle-reinforced AHMMCs [9]. Moreover, EDM is used as a tool in industrial applications such as tank armours, driveshaft, jets landing gear, rotary compressor vane and cylinder liners [10].

Nevertheless, in EDM processing, it is essential to acquire significant machining performances like high MRR, less TWR, low SR, reduced amount of power consumption (PC), minor volume of recast layer/white layer (RCL/WL) thickness and reduced overcut (OC). Moreover, the machining performance is responsively liable upon the input parameters alike pulse current ( $I$ ), voltage ( $V$ ), pulse on time ( $\mu s$ ), pulse off time ( $\mu s$ ) and also the non-electrical properties, i.e., dielectric, tool rotation and work piece rotation [11]. Suresh Kumar et al. [12] define that the larger crater and high surface waviness were produced by intensification in pulse on time and peak current. Riaz Ahmed et al. [13] demarcated

that an extensive duration of spark was crucial with a tremendous value of flushing pressure for high metal removal rate in  $B_4C$ - and SiC-reinforced materials. Hourmand et al. [14] reveal that the current, pulse on time, and voltage have a significant effect on the microstructure of machined surface. Pulse on time affects the surface roughness when copper was used as electrode [15].

Sweety Mahanta et al. [16] defined the most influencing parameters that affect performance measures were current and pulse on time. Kumar and Prakash [17] found the optimal setting of parameters in S/N ratio through Taguchi technique to obtain the best response. To predict the optimal conditions for EDM machining, a mathematical modelling has been developed [18]. Sidhu et al. [19] reported that most of the EDM work has been carried out on matrix phase reinforced with single particulates and only a little amount of researches have been done on matrix phase reinforced with two or more particulates; hence, it is still an open area for research. Hence, in this research work, the EDM machining work has been carried out on matrix phase reinforced with two particulates.

The machined material desires to be in good precision with the best form of tolerance done by EDM process. Moreover, the design created by EDM and tolerances are necessary in manufacturing dies, tools, moulds and press work operation [20]. Furthermore, the goal for the industries is to manufacture precise parts with reasonable cost according to predefined provisions for dimensions and geometry. So, the manifestation of geometrical deviations is mandatory [21]. Henceforth, the geometric tolerance such as circularity (CR), cylindricity (CY), perpendicularity (PP) and radial overcut (ROC) was necessary to improve. Selvarajan et al. [22] optimized the EDM parameters for enhancing the circularity, cylindricity and perpendicularity by employing grey relational analysis technique. Using this method, they have enriched the tolerance. Dhanabalan et al. [23] analysed electrical discharge machining process on the form tolerances and the results direct that while expanding the pulse on time, the value of circularity, cylindricity and perpendicularity decreased up to 350  $\mu s$  and then increased with expanding the pulse on time. Sweety Mahanta et al. [16] investigated that the SR and MRR values increase with a hike in the peak current and pulse on time; moreover, wider and deeper crater was observed due to high melting and vaporization of the material.

In recent scenario, the usage of EDM process is becoming a significant development in modern manufacturing engineering field. Therefore, the utilization of EDM process has to be facilitated by reducing the budget of machining. Accordingly, to decrease the budget of machining, an optimization methodology must be executed. This extant investigational work emphasizes by implementing a grey relational optimization technique to delineate the optimal value of the

input parameter. By performing the grey relational optimization technique, the intended output responses were better responsive for dissimilar materials on various non-conventional machining methods instance EDM [24–29]. Anand et al. [30] have done an investigation of drilling parameters on hybrid polymer composite by utilizing the optimization tools such as GRA, regression, fuzzy logic and ANN models. From this investigation, they concluded that the Taguchi's technique with GRA is the most reliable method for optimizing the process parameters for multi-response characteristics. Hence, in this present work, we have utilized the Taguchi technique with GRA for optimizing.

From the above literature reviews, it seems that no exertion has been done on the hybrid metal matrix composite for enlightening the geometric tolerances. This extant paper presents optimized EDM parameters by grey relational analysis on the aluminium-based hybrid metal matrix composites (AHMMCs) to augment the geometric tolerance such as circularity (CR), cylindricity (CY), perpendicularity (PP) and radial over cut (ROC). The AHMMCs were fabricated through the stir casting approach. Subsequently, the machining of AHMMCs was succeeded by electrical discharge machining (EDM). By handling  $L_{27}$  orthogonal array approach, the input parameter such as peak current ( $I$ ), pulse on time ( $T_{on}$ ) and gap voltage ( $V$ ) was deliberated. The GRA methodology was projected to discover the optimal input parameters for succeeding enhanced output responses. By utilizing the ANOVA analysis, the greatest contributing input parameter was also resolved. Finally, the endorsement test was handled to authorize the optimal input parameters and also the improvement in grey relational grade was resolved. Furthermore, the effect of peak current and pulse on time was analysed through surface plots. Additionally, the microstructure of the machined surface was analysed using SEM and the results were deliberated regarding the effect of peak current, pulse on time and gap voltage.

## 2 Materials and methods

### 2.1 Fabrication of material

Stir casting approach was utilized to create the composite material which consists of Al 4032 alloy as the matrix material. However, the chemical composition of Al 4032 alloy is represented in Table 1. The ceramic materials such as TiC (titanium carbide) and h-BN (hexagonal boron nitride) as reinforcement materials were purchased from M/s Sigma

Aldrich, Germany. Superior mechanical properties explicitly wear resistance and virtuous abrasive resistance were provided by the TiC material. h-BN has virtuous thermal shock resistance and thermal conductivity, tremendous substitute for other ordinarily used lubricants such as graphite, molybdenum di sulphide and oils. Hence, the prepared composite material can be adopted in the application of cylinder liner. Figure 1 a–c shows the SEM image of received materials such as aluminium alloy 4032, TiC and BN, and it illustrates that  $\alpha$ -phase was presented in the aluminium alloy 4032, while TiC and H-BN have face-centred cubic structure, respectively.

Al alloy (4032) scraps were warmed in the casting furnace. Although the reinforcement materials such as 6 wt.% of TiC and 2 wt.% of BN were preheated to a temperature of 1000 °C to eradicate the oxidation. Subsequently, the preheated Al alloy was further heated above its liquescent point and melted completely to obtain the liquidus stage. Furthermore, the liquefied material was cooled slowly to its liquidus temperature. Moreover, the degasser and cover-all powder were further added to the melted liquid, respectively, so as to eradicate the impurities existed in the liquefied metal and to retain the temperature at the innermost of the crucible.

After eradicating the impurities, the preliminary heated reinforcement materials were added into the liquefied material and stirred using an electrical motor with a rapidity of 500 rpm for a precise period of 5–10 min. The stirrer process has been supported for the identical dissemination of reinforcement elements in the molten material. Subsequently, the blended liquefied metal was well preserved at a temperature of 800 °C. Finally, the liquefied metal was transferred into the warmed die having a dimension of 100 mm × 100 mm × 10 mm. The fabricated hybrid composite material was contrived for tensile examination as per ASTM, and the consequences are offered in Table 2.

### 2.2 Machining process

A die-sinking EDM attached with three phase servo stabilizer was deployed for machining the fabricated composite material. Electrolyte copper electrode rod of 10 mm diameter and 80 mm length was handled. The workpiece was kept in the machine bed and connected to the positive polarity, and the electrode is connected to the negative polarity. To weaken the attrition between the tool and the work piece and to clean the debris from the spark gap, a dielectric medium, called EDM oil, was used at a constant pressure of 1.0 kgf/cm<sup>2</sup>. The dielectric fluid was filled in

**Table 1** Chemical composition of Al 4032 alloy

Element	Si	Mg	Fe	Cu	Zn	Ni	Cr	Al
Wt%	11–13.5	0.8–1.3	Max 1.0	0.50–1.3	Max 0.25	0.50–1.3	Max 0.10	Bal

**Fig. 1** SEM image of received. **a** Al alloy 4032, **b** titanium carbide, **c** H–boron nitride

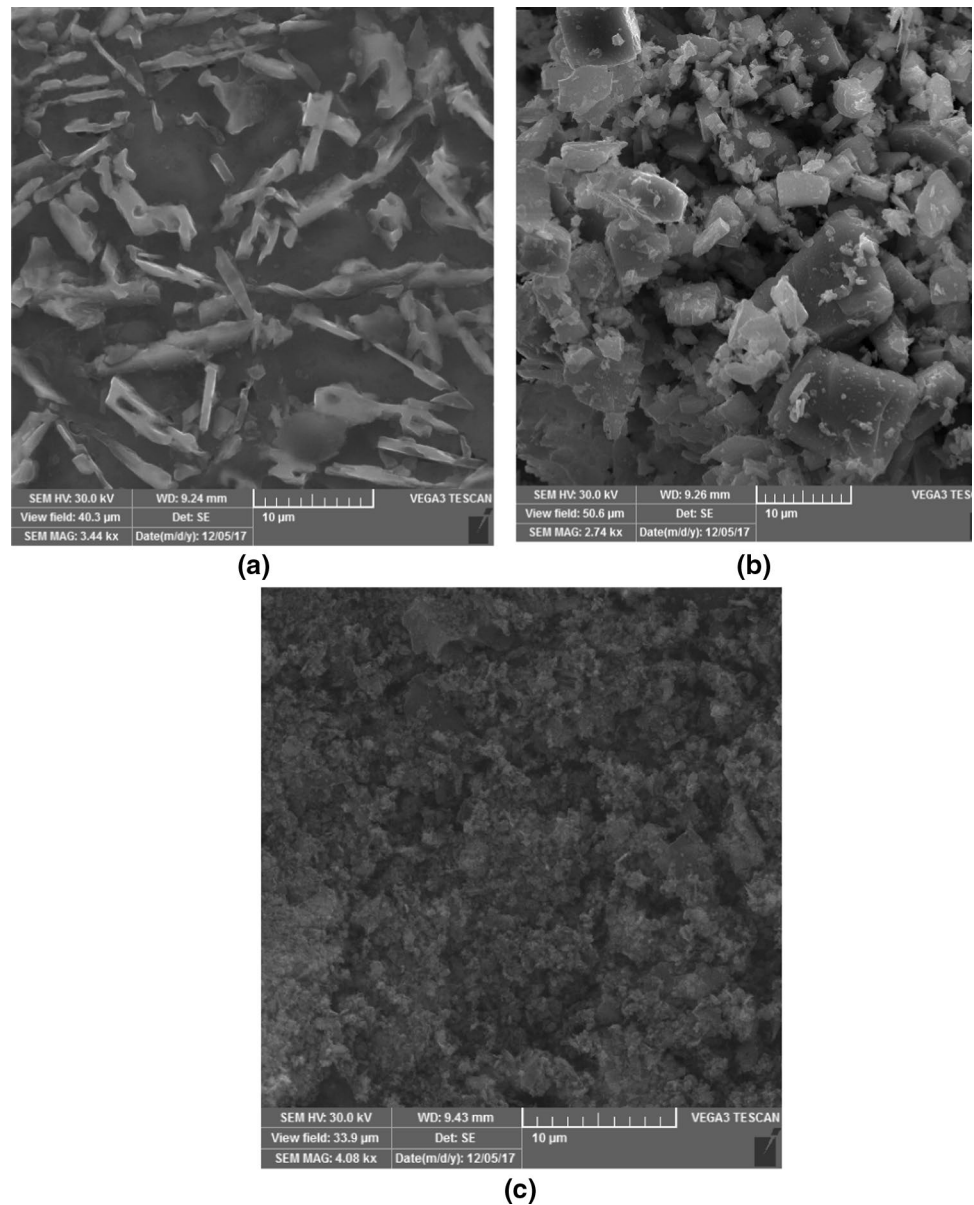


**Table 2** Mechanical properties of the fabricated composite material

Composite	Tensile strength (N/mm <sup>2</sup> )	Yield strength (N/mm <sup>2</sup> )	Density g/cm <sup>3</sup>	Hardness (HV)
Al 4032-6% TiC-2% h-BN	412	341	2.70	145

the closed machined bed until the electrode and the workpiece get immersed by the dielectric medium. EDM system was provided with a dielectric tank to store the dielectric medium, dielectric pump to maintain the level, filter system, a level indicator to check the level of the dielectric medium.

From the literature reviews, it seems that peak current (A) and pulse on time ( $\mu$ s) are two major significant parameters that affect the performance characteristics of the EDM process. A similar observation has been reported by Kumar and Parkash [17]. The gap voltage parameter has little effect on the overcut performance [18]. Although the levels of the parameter were selected based on the literature reviews [12, 18]. Hence, in this research work the parameters like peak current, pulse on time and gap voltage were selected for performing the machining process. The input parameters and their levels are mentioned in Table 3.

By applying  $L_{27}$  orthogonal array procedure on the various input parameters alike peak current (A), pulse on time ( $\mu$ s) and gap voltage (v), the machining process was organized. When the tool and the workpiece gets closer, a



**Table 3** Input parameter and their levels

S. No	Parameters	Level 1	Level 2	Level 3
1	Peak current (A)	9	12	15
2	Pulse on time ( $\mu$ s)	50	75	100
3	Gap voltage (v)	30	35	40

discharge energy was produced between the spark gap and the material was removed from the workpiece due to melting. A hole was produced on the surface of the workpiece about 10 mm in diameter and with a depth of 2 mm. After the material removal process, the dielectric fluid was utilized to flush away the eroded debris. Thus, the machining was carried over for all the experiments.

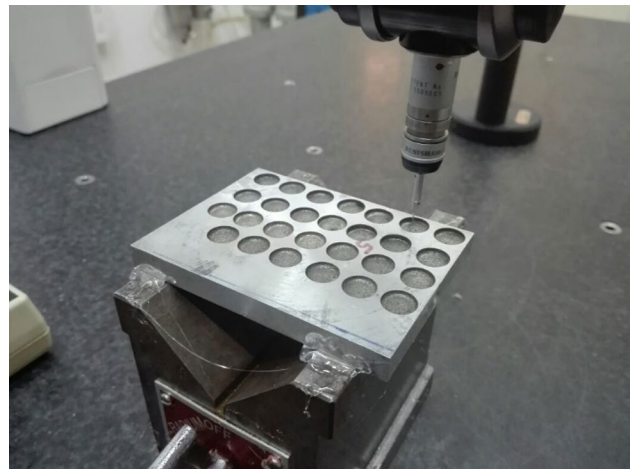
The machined composite material is shown in Fig. 2. From this figure, it illustrates that on the basis of  $L_{27}$  orthogonal array machining have been done on the composite material and it confirms that no deviation has been occurred.

### 2.3 Measurement of output responses

A CNC coordinate measuring machine (CMM) was exploited to quantify the output responses such as circularity (CR), cylindricity (CY), perpendicularity (PP) and radial over cut (ROC).

A circular plane was designated, and the probe of the CMM machine as shown in Fig. 3 was used to measure the circularity of the specimen by tracing the eight different positions.

The probe in the CMM machine was prepared to trace the eight different positions alongside the innermost surface of the selected hole. The circularity and cylindricity were measured with the aid of CALYPSO computing software of the CMM machine.

**Fig. 2** Machined composite material**Fig. 3** A probe in CMM used to measure the tolerances

Perpendicularity was defined as the condition of a surface or line that lie exactly at  $90^\circ$  with respect to the axis. At a constant hole depth, an annotation plane was created by selecting the numeral of points. With esteem to the reference plane from the topmost to bottommost of the pit at variable diametric positions, a limited point was selected.

The difference between the dimension of the electrode tool and hole created on the composite material during machining was determined as the radial overcut (ROC). The measurement of the hole created on the composite material was defined using the CMM machine. The radial overcut was determined by the following empirical relation.

$$ROC = \left[ \frac{D_{hc} - D_{te}}{2} \right] \quad (1)$$

where  $D_{hc}$  is the diameter of the hole created on the machined surface;  $D_{te}$  is the diameter of the tool electrode.

### 2.4 Optimization by grey relational analysis

The grey relational analysis was carried out for the output responses such as circularity, cylindricity, perpendicularity and radial overcut which are in Table 4. To discover the optimal combination of process parameters, a multi-response optimization method, namely the grey relational analysis, was ordinarily inspired in the diverse engineering arenas. Also, using this optimization analysis, the domination of individual process parameter on the output responses was gauged. Additionally, an optimal single grey grade was achieved to examine the multi-performance characteristics. So as to apply the grey relational analysis system for obtaining optimal value of process parameters, the ensuing steps were followed.

**Table 4** Output responses for all the experiments

Experiment no	Peak current (A)	Pulse on time ( $\mu$ s)	Gap voltage (v)	CR (mm)	CY (mm)	PP (mm)	ROC (mm)
1	9	50	30	0.0332	0.0226	0.2782	0.1408
2	9	50	35	0.0152	0.0368	0.1361	0.0919
3	9	50	40	0.0124	0.0285	0.1227	0.0719
4	9	75	30	0.0157	0.0324	0.0674	0.1079
5	9	75	35	0.0162	0.0718	0.1935	0.1426
6	9	75	40	0.0103	0.0729	0.1428	0.1056
7	9	100	30	0.0155	0.0497	0.0674	0.1212
8	9	100	35	0.0207	0.534	0.0795	0.1648
9	9	100	40	0.0013	0.0441	0.0368	0.1326
10	12	50	30	0.0395	0.0314	0.0134	0.0974
11	12	50	35	0.0312	0.0614	0.0579	0.1948
12	12	50	40	0.0183	0.0262	0.0122	0.1466
13	12	75	30	0.0194	0.0841	0.1176	0.1316
14	12	75	35	0.0412	0.0374	0.0337	0.1314
15	12	75	40	0.0793	0.1058	0.0108	0.1328
16	12	100	30	0.0765	0.0592	0.0734	0.1236
17	12	100	35	0.0386	0.0098	0.0074	0.0981
18	12	100	40	0.0197	0.0833	0.1193	0.1146
19	15	50	30	0.0159	0.0397	0.0631	0.1395
20	15	50	35	0.0274	0.1447	0.1793	0.1833
21	15	50	40	0.0086	0.0916	0.1157	0.1933
22	15	75	30	0.0211	0.1429	0.1584	0.1592
23	15	75	35	0.0538	0.096	0.2028	0.1076
24	15	75	40	0.3598	0.0399	0.0876	0.0972
25	15	100	30	0.1009	0.0919	0.0523	0.1827
26	15	100	35	0.5266	0.0654	0.3907	0.1327
27	15	100	40	0.3447	0.1058	0.79	0.1606

#### 2.4.1 Step 1: Calculation of S/N ratio

The signal-to-noise (S/N) ratio analysis was prompted for linking the investigational results. In this research work, a lower values of the machining characteristics such as circularity, cylindricity, perpendicularity and radial overcut are advantageous. Hence, smaller the better response was selected. A smaller S/N ratio was reckoned by exploiting Eq. 2.

$$S/N \text{ ratio} = -10 \log_{10} \left( \frac{1}{n} \right) \sum_{i=1}^n y_{ij}^2 \quad (2)$$

In Eq. 2, where  $n$  is the numeral of repetitions;  $y_{ij}$  = observed response;  $i = 1, 2, \dots, n$ ;  $j = 1, 2, \dots, k$ .  $i$ th response value in the  $j$ th experimentation.  $i$  = numeral of responses, and  $j$  = number of experiments.

#### 2.5 Step 2: Calculation of normalization

The response values have to be normalized formerly by scrutinizing them with the grey relational model. In this work, the normalization was accomplished for individual experiments. The output responses such as circularity, cylindricity, perpendicularity and radial overcut are to be minimized. Hence, for diminishing the performance characteristics Eq. 3 was applied to estimate the normalized values of experimental outcomes.

$$X_{ij} = \frac{\max(y_{ij}, i = 1, 2, \dots, n) - y_{ij}}{\max(y_{ij}, i = 1, 2, \dots, n) - \min(y_{ij}, i = 1, 2, \dots, n)} \quad (3)$$

where  $y_{ij}$  the  $i$ th performance characteristics in the  $j$ th experiment, and  $\max y_{ij}$  and  $\min y_{ij}$  are the maximal and diminutive

values of the  $i$ th performance characteristics for substitute the experimentation.

## 2.6 Step 3: Estimation of deviance sequence

Before the valuation of the grey relational coefficient, the examination of deviation sequence was mandatory. A reference sequence ( $X_0$ ) and pursuance sequence ( $X_{ij}$ ) were necessary for the estimation of deviation sequence. The deviation sequence was reckoned from Eq. 4.

$$\Delta_{0j}(k) = |X_0(k) - X_{ij}(k)| \quad (4)$$

where  $X_{ij}$  is the  $j$ th performance characteristics in the  $i$ th value of normalization and for  $X_0$  the reference value of 1 was fixed for all the experiments.

## 2.7 Step 4: Computation of grey relational coefficient

The grey relational coefficient (GRC) was calculated by executing the assessment of deviance sequence in Eq. 5.

$$(y_0(k), y_i(k)) = \frac{\Delta_{\min} + \xi \Delta_{\max}}{\Delta_{0j}(k) + \xi \Delta_{\max}} \quad (5)$$

where

- i.  $j = 1, 2, \dots, n$ ;  $n = 1, 2, \dots, m$ , is the numeral of investigational record values and is the numeral of responses;
- ii.  $y_0(k)$  is the quoted array ( $y_0(k) = 1, k = 1, 2, \dots, m$ );  $y_j(k)$  is the precise comparison array;
- iii.  $\Delta_{0j} = ||y_0(k) - y_j(k)||$  is the infinite importance of the disparity betwixt  $y_0(k)$  and  $y_j(k)$ ;
- iv.  $\Delta_{\min} = \min \min ||y_0(k) - y_j(k)||$  is the lowermost value of  $y_j(k)$ ;
- v.  $\Delta_{\max} = \max \max ||y_0(k) - y_j(k)||$  is the uppermost value of  $y_j(k)$ ;
- vi.  $\xi$  defines the range between  $0 \leq \xi \leq 1$  which determines the differentiate of coefficient.

### 2.7.1 Step 5: Evaluation of grey relational grade

To rank the regularity of the experimented value, the grey relational grade (GRG) was estimated by equating the grey relational coefficient for all the outcomes. The grade measure was evaluated exploiting Eq. 6.

$$\delta_j = \frac{1}{k} \sum_{i=1}^m y_{ij} \quad (6)$$

where  $\delta_j$  is the grey relational grade for the  $j$ th examined value and  $k$  is the numeral of performance characteristics.

## 3 Results and Discussion

### 3.1 Microstructure of composite material

The microstructure analysis was carried out on the prepared composite material by the scanning electron microscope and is shown in Fig. 4a. From the figure, it was defined that the microstructure contains a solid solution of Al 4032 alloy and an inter-dendrites network of eutectic aluminium–silicon. Also, it reveals that the reinforcement materials were distributed homogeneously in the matrix alloy and porosity was not presented in the fabricated composite material.

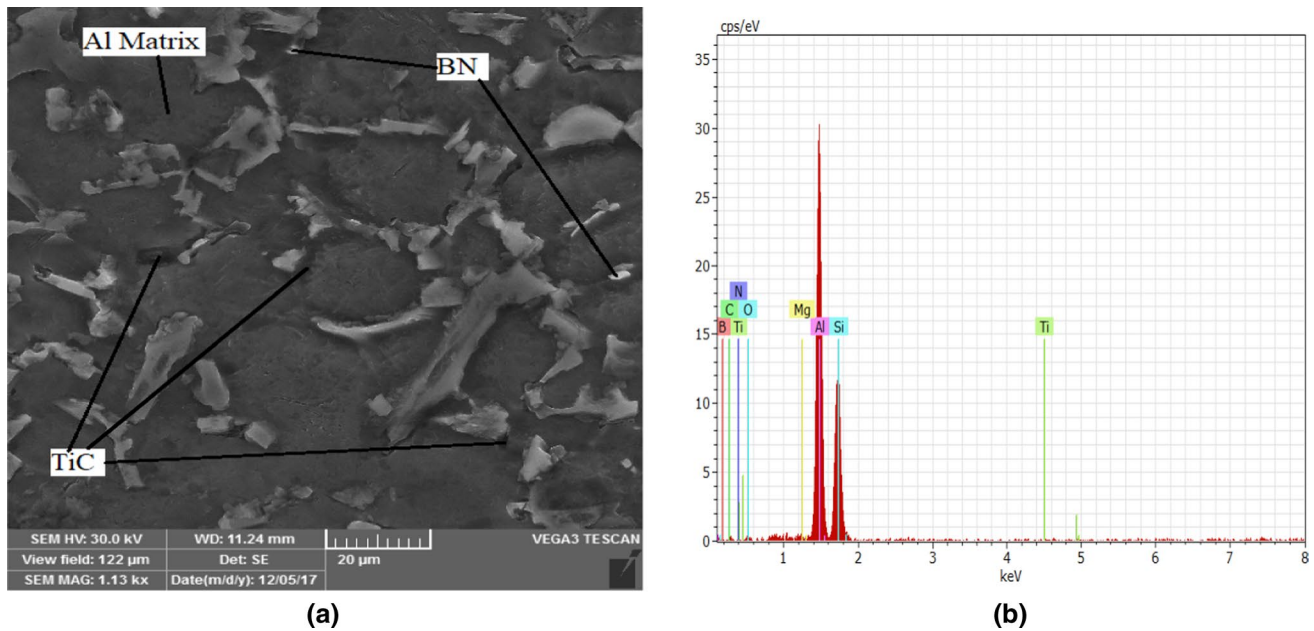
EDS analysis of the composite material was also carried out, and the results are shown in Fig. 4b. The figure confirms a high-intensity peak of aluminium and low-intensity peak of silicon, whereas the chemical composition of aluminium alloy 4032, namely Mg content was also presented in the EDS analysis with a smaller peak. The EDS analysis also confirms that the reinforcement elements such as Ti, C, B and N were presented with a strong peak.

Figure 5a shows that SEM with EDS mapping of Al 4032/TiC/BN composite. From the figure, it reveals that the secondary particles have been evenly distributed in the matrix material after stir casting process. It has ascertained the corresponding EDS analysis.

Figure 5b shows that elemental mapping of Al 4032/TiC/BN composite. Figure reveals that the elements such as Al and Si particle were observed, whereas Mg which is the constituent of base metal Al 4032 was present in little amount. From the spectrum, it has been asserted that B, N, Ti and C have successfully incorporated in the matrix (Al 4032). Figure 5c displays the EDS analysis, and it is also inferred that high-intensity, medium-intensity and low-intensity peaks represent the deviation of the secondary particles, respectively. The map overlay of all elements shows the presence of various colours such as green, red, violet and purple, respectively. It is also inferred that there are some areas where those elements are not combinations with any of the others.

### 3.2 Grey relational grade models

The output response for all experimental value is presented in Table 4. From this experimental value, the S/N ratio and normalization values were performed and are represented in Table 5. The grey relational coefficient and the grey relational grade for the output responses are offered in Table 6. Generally, the predominant value of the grey relational grade was reflected as the superior output responses. From the grey relational grade, it was well defined that the



**Fig. 4** **a** SEM analysis of Al4032-6%TiC-2% h-BN composite material, **b** EDS of Al Al4032-6%TiC-2% h-BN composite material

input parameters such as peak current at 9 A, pulse on time 50 μs and gap voltage at 40 V produced enhanced output performance.

Figure 6 represents the grey relational grade for all the experimentation runs; from the figure, it reveals that the experimentation number 3 shows greater grey relational grade result of 0.9163.

### 3.3 Response table for grey relational grade

Table 7 shows that the average value of the grey relational grade for the discrete parameter at diverse levels was characterized. Further, the response table shows the optimal conditions for discrete parameter and also the foremost consequence of discrete parameter was determined. As the optimum level which was identified from the response table (peak current = 12 A, pulse on time = 50 μs, gap voltage = 30 V) was considered as predicted condition.

### 3.4 ANOVA table

It is necessary to discover the impression of the discrete parameter that affects the combined responses. The optimum status result obtained from the single optimization technique cannot discover the significant parameter on all the process. Hence, an analysis of variance (ANOVA) is an arithmetic tool was handled to categorize the significant parameter and to define the involvement of discrete parameter on the multi-objective parameters.

The ANOVA results are demonstrated in Table 8 which indicates that the peak current contributes more with **69.08%** followed by pulse on time with **19.55%** and gap voltage with **5.69%**.

### 3.5 Authentication Test

To verify the optimum status which was obtained from the response table and also to estimate the progress in the grey relational grade, an authentication test was directed. While using the optimum conditions, the improvement grade for predicted condition and experimental condition is identified in Table 9. The improvement grade for the experimental grey relational grade is high when likened to the anticipated condition with a noteworthy increase of 0.1452. Hence, the inspected outcome was authorized by optimizing the input parameter using GRA.

### 3.6 Influence of current and pulse on time on the output responses

From the response table and ANOVA, it was recognized that the current was the utmost influenced parameter followed by pulse on time on the output responses when likened to the other parameters. The effect of current and pulse on time on geometric tolerances has been explained and is displayed in Figs. 7 and 8. Figures 7 and 8 indicate that as the peak current and pulse on time elevate, the circularity increases throughout the range. Because more discharge energy was created at huge pulse current which guides to increase excess



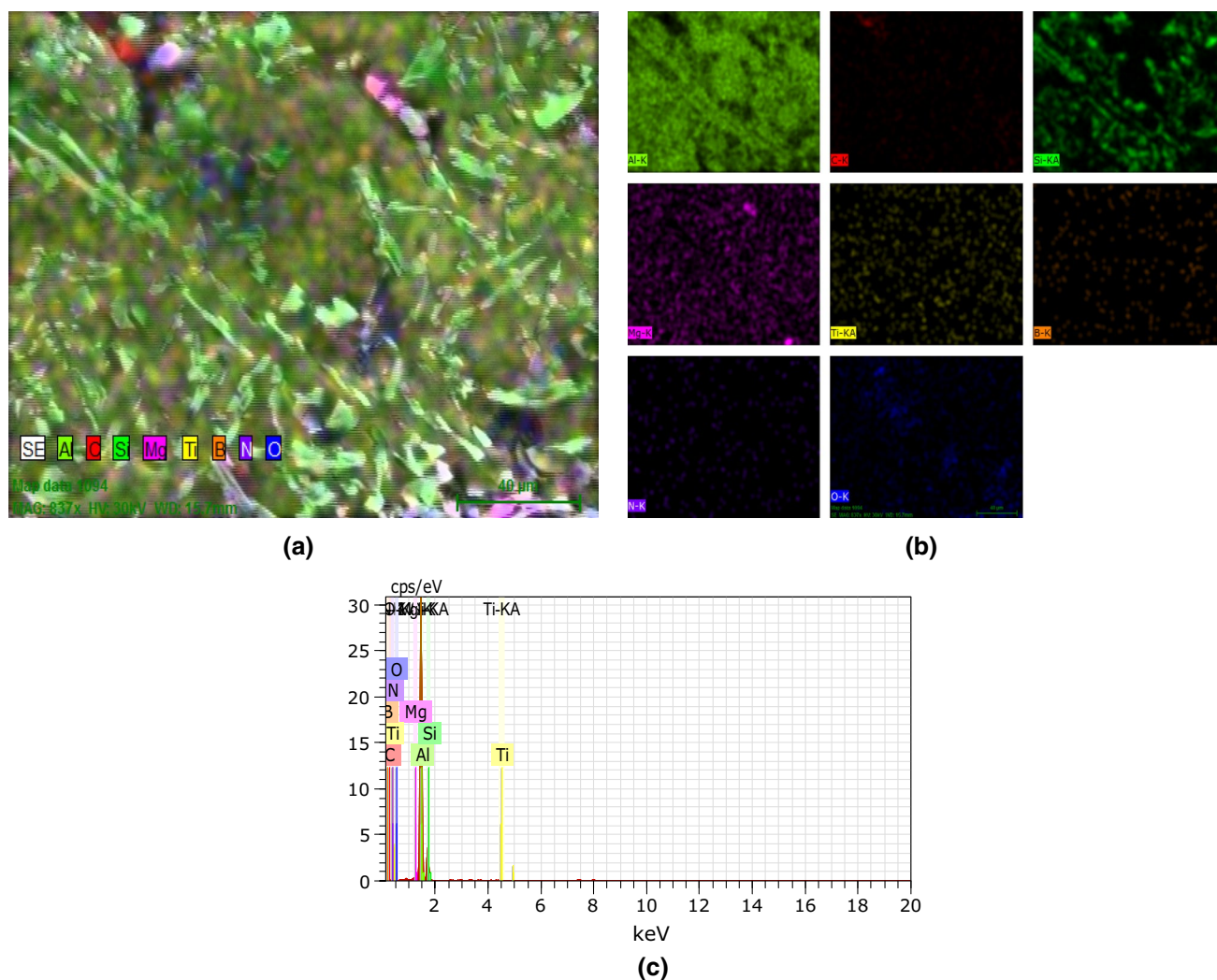


**Fig. 5** **a** SEM with EDS mapping of Al4032-6%TiC-2% h-BN composite, **b** elemental mapping of Al4032-6%TiC-2% h-BN composite, **c** EDS analysis of Al4032-6%TiC-2% h-BN composite

elimination of material. In order to accomplish a diminished circularity, the peak current must be reduced.

Initially, the cylindricity and the perpendicularity decrease with the escalation in current and then by further increasing the current, it augments as exposed in Fig. 7. But the cylindricity and the perpendicularity increases with amplifying the pulse on time as displayed in Fig. 8. This was owed that the duration of spark energy amplified between the workpiece and tool electrode at high pulse on time which permits the vaporization and melting the material from the work piece surface. Hence, at the combination of elevated peak current and pulse on time the cylindricity and perpendicularity gets augmented. A minor cylindricity deviation was succeeded at elevated peak current and at lower pulse on time.

The overcut responses increase with increasing the peak current as shown in Fig. 7. This was likely because while

enhancing the peak current, a higher discharge energy was produced which is responsible for amplifying the overcut. Moreover, huge peak current leads to amplification of pits and dissipates on the machined composite material surfaces. At a lower level of peak current, controlled erosion of material was achieved and provides zero damage around the periphery of the machined hole. The effect of overcut on pulse on time is demonstrated in Fig. 8. From this figure, it explains that the overcut response gets decreased from 50 to 75 μs but additionally increasing the pulse on time from 75 to 100 μs the overcut. This may be attributed to that the heating and melting will be more at high pulse on time and hence the overcut gets enlarged.

**Table 5** The value of S/N ratio and normalization for all the experiments

Experiment no	S/N ratio				Normalization			
	CR	CY	PP	ROC	CR	CY	PP	ROC
1	29.5772	32.9178	11.1129	17.0279	0.9393	0.9756	0.6540	0.4394
2	36.3631	28.6830	17.3228	20.7384	0.9735	0.9485	0.8355	0.8377
3	38.1316	30.9031	18.2231	22.8654	0.9789	0.9643	0.8527	1.0000
4	36.0820	29.7891	23.4268	19.3396	0.9726	0.9569	0.9233	0.7071
5	35.8097	22.8775	14.2664	16.9207	0.9716	0.8817	0.7622	0.4251
6	39.7433	22.7454	16.9054	19.5308	0.9829	0.8796	0.8270	0.7262
7	36.1934	26.0729	23.4268	18.3299	0.9730	0.9239	0.9233	0.5989
8	33.6806	5.4492	21.9927	15.6635	0.9631	0.0000	0.9079	0.2445
9	57.7211	27.1112	28.6830	17.5524	1.0000	0.9346	0.9624	0.5065
10	28.0681	30.0614	37.4579	20.2288	0.9273	0.9588	0.9923	0.7925
11	30.1169	24.2366	24.7464	14.2082	0.9431	0.9016	0.9355	0.0000
12	34.7510	31.6340	38.2728	16.6803	0.9676	0.9687	0.9939	0.3926
13	34.2440	21.5041	18.5919	17.6149	0.9655	0.8583	0.8592	0.5142
14	27.7021	28.5426	29.4474	17.6281	0.9240	0.9473	0.9664	0.5159
15	22.0145	19.5103	39.2754	17.5360	0.8515	0.8169	0.9956	0.5045
16	22.3268	24.5536	22.6861	18.1596	0.8568	0.9058	0.9157	0.5793
17	28.2683	40.1755	42.6154	20.1666	0.9290	1.0000	1.0000	0.7868
18	34.1107	21.5871	18.4672	18.8201	0.9650	0.8598	0.8570	0.6530
19	35.9721	28.0242	23.9994	17.1085	0.9722	0.9430	0.9288	0.4500
20	31.2450	16.7906	14.9284	14.7368	0.9503	0.7427	0.7803	0.0936
21	41.3100	20.7621	18.7333	14.2754	0.9861	0.8440	0.8616	0.0122
22	33.5144	16.8994	16.0049	15.9611	0.9623	0.7461	0.8071	0.2897
23	25.3844	20.3546	13.8586	19.3678	0.9001	0.8356	0.7503	0.7099
24	8.8788	27.9805	21.1499	20.2467	0.3175	0.9426	0.8975	0.7941
25	19.9222	20.7337	25.6300	14.7652	0.8104	0.8434	0.9426	0.0985
26	5.5704	23.6884	8.1631	17.5426	0.0000	0.8939	0.5102	0.5053
27	9.2512	19.5103	2.0475	15.8878	0.3463	0.8169	0.0000	0.2787

### 3.7 Effects of current and pulse on time by surface plots

In order to understand the effect of current and pulse on time on the geometrical tolerances, the 3D surface plots are denoted in Fig. 9a–d. Figure 9a reveals that the circularity increases with amplifying the peak current with a constant pulse on time at both the lower level and higher level. Also, it explains that the circularity range is same as for the pulse on time with constant peak current at both lower level and higher level. Additionally, Fig. 9a shows two different colours specifically blue colour for lower value and green colour for higher value. A lower value of circularity was attained at the combination of low pulse current and low pulse on time.

The effect of peak current and pulse on time on the cylindricity was shown in Fig. 9b. It shows that as the peak current enhances there was a minor change in cylindricity. But the cylindricity enlarges with intensifying the pulse on time at both lower and higher level of peak current. At

a combination of lower level of pulse current and pulse on time, the cylindricity was reduced. Furthermore, Fig. 9b indicates the lower value of cylindricity in blue colour.

The effect of peak current and pulse on time on the perpendicularity is shown in Fig. 9c. It shows that as the peak current increases, the perpendicularity also increases. The value of perpendicularity was low at the combination of low pulse current and low pulse on time. Moreover, Fig. 9c explains that the perpendicularity intensifies more with increasing the pulse on time when compared to the peak current. Correspondingly, the dark blue colour denotes for lower value and light blue for higher value of perpendicularity as shown in Fig. 9c.

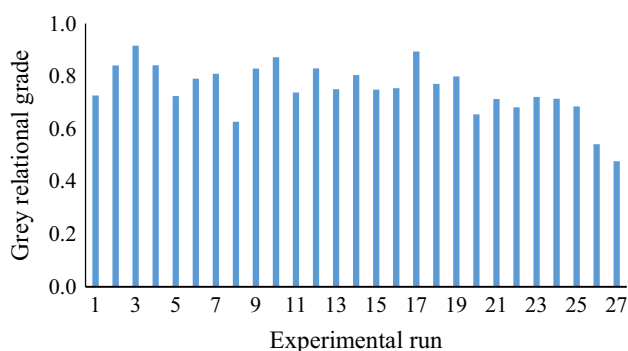
Figure 9d indicates that the overcut expands with augmenting the peak current at both lower level and higher level of pulse on time. At a lower level of peak current and lower value of pulse on time, minimum overcut was obtained. Also, the overcut increases with increasing the pulse on time with constant lower and higher level of peak current.

**Table 6** Grade relational coefficient and grade relational grade

Experiment no	GRC				GRG	Rank
	CR	CY	PP	ROC		
1	0.8917	0.9534	0.5910	0.4714	0.7269	17
2	0.9497	0.9066	0.7525	0.7549	0.8409	5
3	0.9595	0.9334	0.7724	1.0000	0.9163	1
4	0.9480	0.9206	0.8671	0.6306	0.8416	4
5	0.9463	0.8087	0.6777	0.4652	0.7245	18
6	0.9669	0.8060	0.7429	0.6462	0.7905	11
7	0.9487	0.8679	0.8671	0.5549	0.8096	8
8	0.9312	0.3333	0.8444	0.3983	0.6268	25
9	1.0000	0.8843	0.9301	0.5033	0.8294	7
10	0.8730	0.9239	0.9849	0.7067	0.8721	3
11	0.8978	0.8355	0.8857	0.3333	0.7381	16
12	0.9392	0.9411	0.9879	0.4515	0.8299	6
13	0.9355	0.7791	0.7803	0.5072	0.7505	14
14	0.8681	0.9047	0.9370	0.5081	0.8045	9
15	0.7710	0.7319	0.9912	0.5022	0.7491	15
16	0.7774	0.8414	0.8557	0.5431	0.7544	13
17	0.8756	1.0000	1.0000	0.7011	0.8942	2
18	0.9345	0.7810	0.7776	0.5903	0.7709	12
19	0.9473	0.8976	0.8754	0.4762	0.7991	10
20	0.9096	0.6602	0.6948	0.3555	0.6550	24
21	0.9730	0.7621	0.7832	0.3361	0.7136	21
22	0.9299	0.6632	0.7216	0.4131	0.6819	23
23	0.8334	0.7525	0.6670	0.6329	0.7214	19
24	0.4228	0.8970	0.8299	0.7084	0.7145	20
25	0.7251	0.7615	0.8971	0.3567	0.6851	22
26	0.3333	0.8250	0.5052	0.5027	0.5415	26
27	0.4334	0.7319	0.3333	0.4094	0.4770	27

### 3.8 Microstructure analysis on machined surface

The microstructure analysis on the machined surface was done successfully using the scanning electron microscope. Figure 10a–c shows the microstructure of the EDMed surface at different input parameters. Figure 10a displays the machined surface at  $I=9$  A;  $T_{on}=50$   $\mu$ s;  $V=30$  V. From

**Fig. 6** Grey relational grade

this figure, it reveals that the surface was smooth and even. Microcracks were absent at low pulse current and low pulse on time. Less number of microvoids and craters were generated in the machined surface irrespective of the low pulse current, low discharge energy was produced, and less plasma channels were produced. Furthermore, at low pulse on time the duration of discharge energy was less; hence, low material was removed and also smoother surface was produced. Likewise, at the lower level of gap voltage, a better accuracy and surface finish was achieved. Because at the combination of lower level peak current, pulse on time and gap voltage, less spark energy was generated which leads to a decrease in the removal of metal from the workpiece.

Figure 10b illustrates the machined surface at  $I=12$  A;  $T_{on}=75$   $\mu$ s;  $V=35$  V. Figure 10b demarcates that more microvoids and crater were formed as compared to Fig. 10a and also the size of the crater and voids was augmented. This was due to that as the pulse current increases the size of the microvoids and crater was amplified. However, more plasma energy was created at high pulse current and also the circularity of the machined hole was increased. As

**Table 7** Response table for grey relational rank

Parameter	Grey relational grade			Optimum level	Main effect (max–min)	Rank
	Level 1	Level 2	Level 3			
Peak current (A)	0.7896	0.7960	0.6655	2	0.1305	1
Pulse on time (μs)	0.7880	0.7532	0.7099	1	0.0781	2
Gap voltage (v)	0.7690	0.7274	0.7546	1	0.0416	3
Error	0.7461	0.7317	0.7733	3	0.0416	
Total mean value of the grey relational grade = 0.7504						

**Table 8** ANOVA table

Source	DF	SS	MS	F-value	Contribution (%)
Peak current (A)	2	0.0325	0.0162	121.5721	69.08
Pulse on time (μs)	2	0.0092	0.0046	34.4035	19.55
Gap voltage (v)	2	0.0027	0.0013	10.0149	5.69
Error	20	0.0027	0.0001		5.68
Total	26	0.0470	0.0018		

**Table 9** Authentication result

Optimum level	Initial parameter $I=9\text{ A}; T_{on}=50\text{ }\mu\text{s}; V=30\text{ v}$	Predicted parameter $I=12\text{ A}; T_{on}=50\text{ }\mu\text{s}; V=30\text{ v}$	Experimental parameter $I=12\text{ A}; T_{on}=50\text{ }\mu\text{s}; V=30\text{ v}$
Grey relational grade	0.7269	0.8523	0.8721
Improvement in grade	–	0.1254	0.1452

piece surface and develops the creation of cavity in the machined surface.

The machined surface at  $I=15\text{ A}; T_{on}=100\text{ }\mu\text{s}; V=40\text{ V}$  is shown in Fig. 10c. More number of microvoids and crater are presented in Fig. 10c when matched to Fig. 10a, b. The size of the crater was enlarged at the condition of  $I=15\text{ A}$ . This was owed to that when the current was amplified, a large amount of heat energy was instigated which causes poor surface finish. The average size of the microvoids was high at the condition of  $I=15\text{ A}$

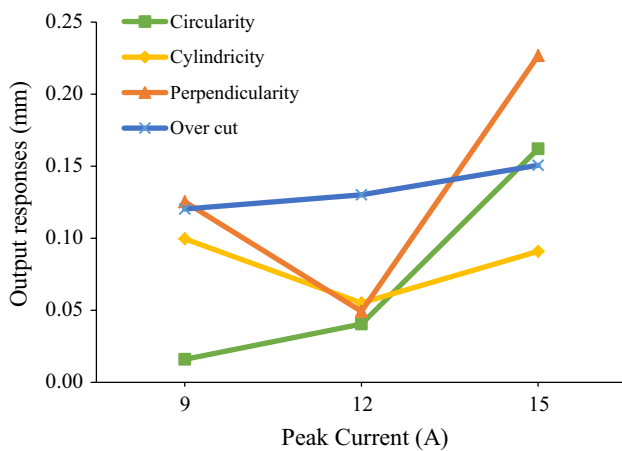


**Fig. 7** Influence of peak current on the output responses

the pulse on time increases a prolonged discharge energy was spawned at the spark gap which leads to the development of micro cracks demonstrated in Fig. 10b. Moreover, the crater formation was big in size when compared to Fig. 10a. This was attributed to that as the pulse on time increases, the period of discharge energy increases, which permits the elimination of excess material from the work

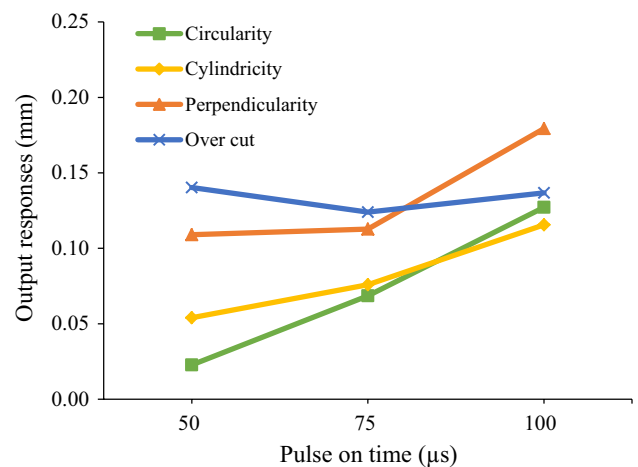


**Fig. 8** Influence of pulse on time on the output responses

when likened to the condition of  $I=12\text{ A}$ . And also at the condition of  $I=15\text{ A}$ , the geometric tolerances such as circularity, cylindricity and perpendicularity were increased; because of higher pulse current, more plasma channels were created on the surface of the work piece which leads



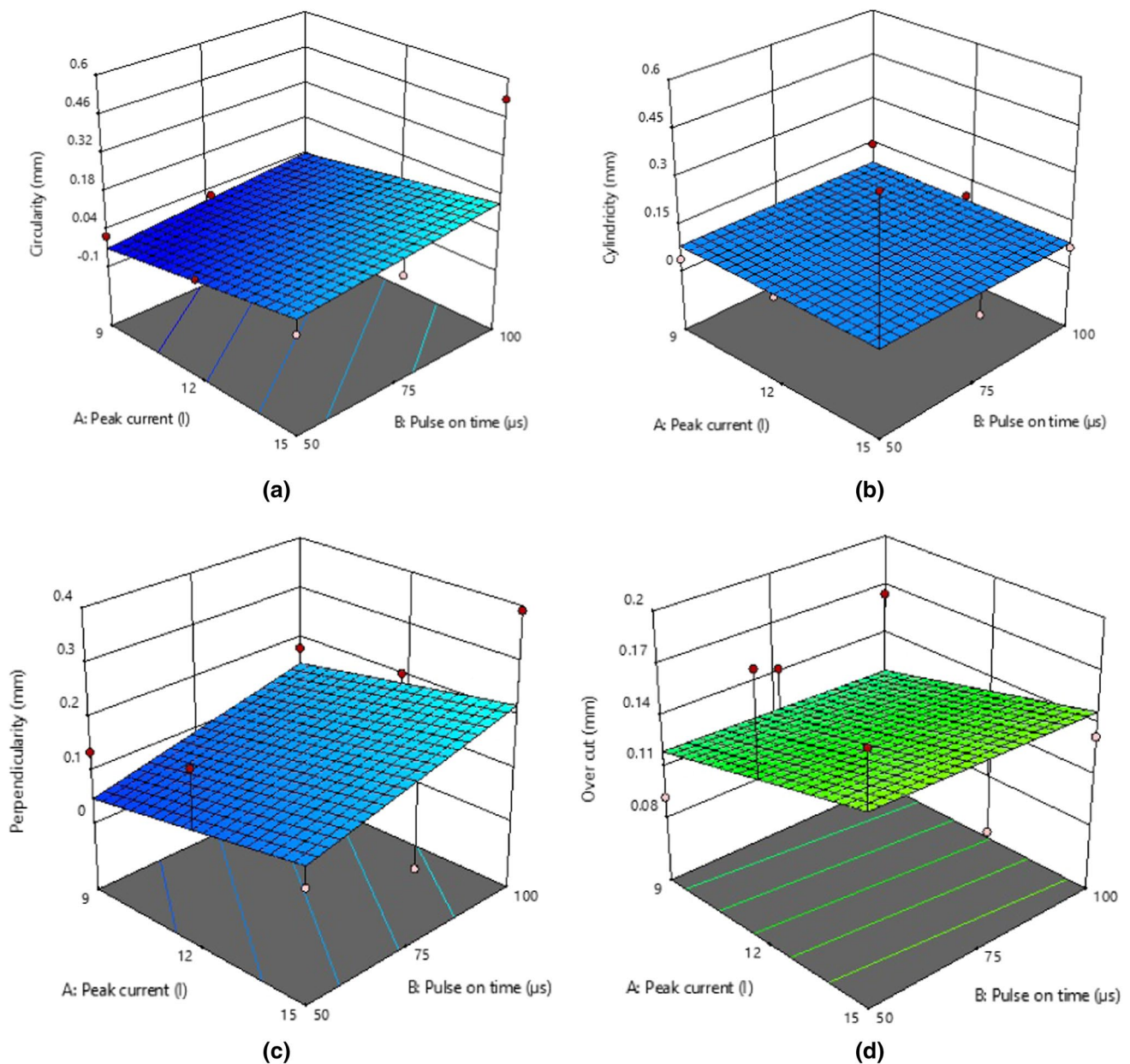


**Fig. 9** Surface plots for **a** circularity versus peak current and pulse on time, **b** cylindricity versus peak current and pulse on time, **c** perpendicularity versus peak current and pulse on time, **d** overcut versus peak current and pulse on time

to removal of huge amount of material, and the crack density was developed in the condition of  $I = 15$  A compared to  $I = 12$  A. As the peak current elevates, a high thermo-electric energy was created at the spark gap. Moreover, it affects the surface appearances of the work piece material. A related statement was denoted by Suresh kumar et al. [31]. Moreover, at high pulse on time, there was an increase in density of microcracks. This was because at high pulse on time the ultimate stress of the composite materials was exceeded by the stress that occurred on the machined surface which leads to the development

of microcracks. Consequently, the size of the crater and microvoids was further augmented with amplifying the pulse on time because the duration of discharge energy was more at high pulse on time. Likewise, at high gap voltage, the machined surface was poor. This result was ascribed to that after high gap voltage prolonged spark energy was created and it affects the surface finish. At the conditions  $I = 15$  A,  $T_{\text{on}} = 100$   $\mu\text{s}$  and  $V = 40$  V, a high blasting force was generated which affects the surface characteristics. Furthermore, the uneven machined surface was realized when related to the remaining two conditions.

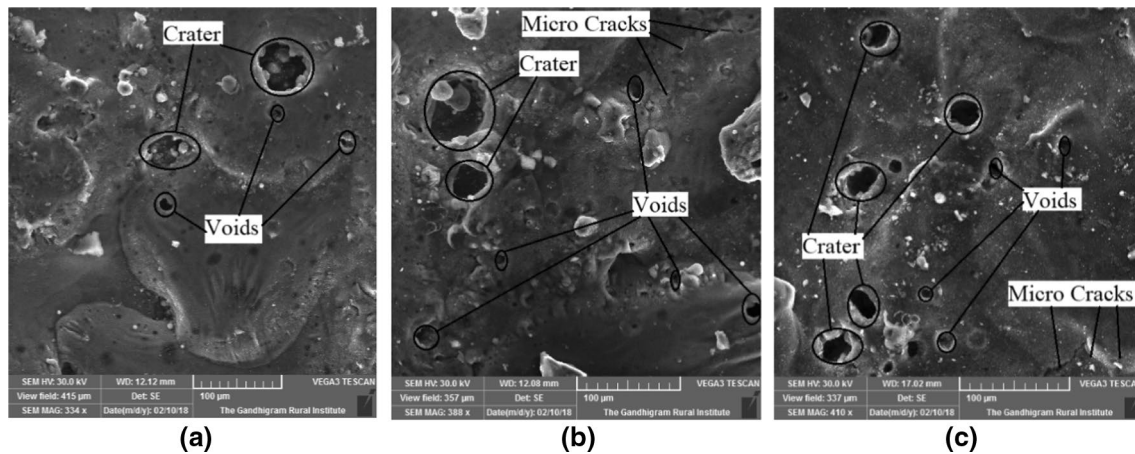


**Fig. 10** Machined surface of Al4032-6%TiC-2% h-BN composite at. **a**  $I=9\text{ A}$ ;  $T_{\text{on}}=50\ \mu\text{s}$ ;  $V=30\ \text{V}$ , **b**  $I=12\text{ A}$ ;  $T_{\text{on}}=75\ \mu\text{s}$ ;  $V=35\ \text{V}$ , **c**  $I=15\ \text{A}$ ;  $T_{\text{on}}=100\ \mu\text{s}$ ;  $V=40\ \text{V}$

## 4 Conclusions

The aluminium hybrid composite material was primed successfully by the stir casting approach, and the material was machined effectively by electrical discharge machining route with different input parameters that influence the output responses. By handling the grey relational analysis tool, the output responses were optimized and the succeeded conclusions were obtained:

1. The optimal conditions alike peak current of 12 A, pulse on time of 50  $\mu\text{s}$  and gap voltage of 30 V were attained through grey relational analysis for attaining minor deviation in circularity, cylindricity, perpendicularity and radial overcut.
2. The optimum conditions acquired from the response table ( $I=12\ \text{A}$ ;  $T_{\text{on}}=50\ \mu\text{s}$ ;  $V=30\ \text{V}$ ) were deliberated as the anticipated parameter, and it resembled the 10th experimental condition.
3. Authentication test exemplified that the improvement in the grey relational grade value of experimental conditions has a noteworthy increase of 0.1452 and 0.0198 when likened to the initial parameter and the predicted parameter.
4. Noteworthy contribution parameter was manifested by the ANOVA table and resulted that contribution of current is **69.08%**.
5. The circularity and radial overcut of the machined surface distended with an increase in peak current throughout its range. The cylindricity deviation was decreased with a combination of elevated peak current and lower pulse on time.
6. Surface characteristics were fruitfully examined by the scanning electron microscope. The average size of the microvoids was high at the condition of  $I=15\ \text{A}$  when

compared to the condition of  $I=12\ \text{A}$ . The machined surface at conditions  $I=15\ \text{A}$ ,  $T_{\text{on}}=100\ \mu\text{s}$  and  $V=40\ \text{V}$  was uneven when compared to the remaining two conditions.

## 5 Future work

- The flushing pressure of the dielectric medium will also be considered for optimization.
- The output responses such as MRR, TWR and SR will be analysed.
- The machining of HAMMCs will be done through wire-EDM, and the effect of geometric tolerances will be studied.

## References

1. Karl UK (2006) Metal matrix composites custom-made materials for automobile and aerospace engineering. <https://doi.org/10.1002/3527608117>
2. Chawla KK, Chawla N (2014) Metal matrix composites: automotive applications. Encycl Automot Eng. <https://doi.org/10.1002/9781118354179.auto279>
3. Nikhilesh C, Krishan K (2006) Metal matrix composites. Springer, London. <https://doi.org/10.1007/978-1-4614-9548-2>
4. Clyne TW, Withers PJ (2014) An introduction to metal matrix composites. <https://doi.org/10.1007/s13398-014-0173-7.2>
5. Thirumalai Kumaran S, Uthayakumar M (2014) Investigation on the dry sliding friction and wear behaviour of AA6351-SiC-B<sub>4</sub>C hybrid metal matrix composites. Proc Inst Mech Eng Part J J Eng Tribol 228(3):332–338. <https://doi.org/10.1177/1350650113508103>
6. Alam MT, Ansari AH, Arif S, Alam MN (2017) Mechanical properties and morphology of aluminium metal matrix

- nanocomposites-stir cast products. *Adv Mater Process Technol* 698(July):1–16. <https://doi.org/10.1080/2374068X.2017.1350543>
7. Ho KH, Newman ST (2003) State of the art electrical discharge machining (EDM). *Int J Mach Tools Manuf* 43(13):1287–1300. [https://doi.org/10.1016/S0890-6955\(03\)00162-7](https://doi.org/10.1016/S0890-6955(03)00162-7)
  8. Pramanik A (2014) Developments in the non-traditional machining of particle reinforced metal matrix composites. *Int J Mach Tools Manuf* 86:44–61. <https://doi.org/10.1016/j.ijmactool.2014.07.003>
  9. Jameson EC (2001) Electric discharge machining. Society of Manufacturing Engineers, Dearborn
  10. Garg RK, Singh KK, Sachdeva A, Sharma VS, Ojha K, Singh S (2010) Review of research work in sinking EDM and WEDM on metal matrix composite materials. *Int J Adv Manuf Technol* 50(5–8):611–624. <https://doi.org/10.1007/s00170-010-2534-5>
  11. Kandpal BC, kumar J, Singh H (2015) Machining of Aluminium metal matrix composites with electrical discharge machining—a review. *Mater Today Proc* 2(4–5):1665–1671. <https://doi.org/10.1016/j.matpr.2015.07.094>
  12. Kumar SS, Uthayakumar M, Kumaran ST, Parameswaran P (2014) Electrical discharge machining of Al(6351)–SiC–B<sub>4</sub>C hybrid composite. *Mater Manuf Process* 29(11–12):1395–1400. <https://doi.org/10.1080/10426914.2014.952024>
  13. Ahamed AR, Asokan P, Aravindan S (2009) EDM of hybrid Al–SiC<sub>p</sub>–B<sub>4</sub>C<sub>p</sub> and Al–SiC<sub>p</sub>–glassp MMCs. *Int J Adv Manuf Technol* 44(5–6):520–528. <https://doi.org/10.1007/s00170-008-1839-0>
  14. Hourmand M, Farahany S, Sarhan AAD, Noordin MY (2015) Investigating the electrical discharge machining (EDM) parameter effects on Al–Mg<sub>2</sub>Si metal matrix composite (MMC) for high material removal rate (MRR) and less EWR–RSM approach. *Int J Adv Manuf Technol* 77(5–8):831–838. <https://doi.org/10.1007/s00170-014-6491-2>
  15. Mathai VJ, Dave HK, Desai KP (2017) Experimental investigations on EDM of Ti6Al4 V with planetary tool actuation. *J Braz Soc Mech Sci Eng* 39(9):3467–3490. <https://doi.org/10.1007/s40430-016-0657-9>
  16. Mahanta S, Chandrasekaran M, Samanta S, Arunachalam RM (2018) EDM investigation of Al 7075 alloy reinforced with B<sub>4</sub>C and fly ash nanoparticles and parametric optimization for sustainable production. *J Braz Soc Mech Sci Eng*. <https://doi.org/10.1007/s40430-018-1191-8>
  17. Kumar P, Parkash R (2016) Experimental investigation and optimization of EDM process parameters for machining of aluminum boron carbide (Al–B<sub>4</sub>C) composite. *Mach Sci Technol* 20(2):330–348. <https://doi.org/10.1080/10910344.2016.1168931>
  18. Dhar S, Purohit R, Saini N, Sharma A, Kumar GH (2007) Mathematical modeling of electric discharge machining of cast Al–4Cu–6Si alloy–10wt.% SiCP composites. *J Mater Process Technol* 194(1–3):24–29. <https://doi.org/10.1016/j.jmatprotec.2007.03.121>
  19. Sidhu SS, Batish A, Kumar S (2013) Fabrication and electrical discharge machining of metal-matrix composites: a review. *J Reinf Plast Compos* 32(17):1310–1320. <https://doi.org/10.1177/0731684413489366>
  20. Selvarajan L, Manohar M, Udhaya kumar A, Dhinakaran P (2017) Modelling and experimental investigation of process parameters in EDM of Si<sub>3</sub>N<sub>4</sub>-TiN composites using GRA-RSM. *J Mech Sci Technol* 31(1):111–122. <https://doi.org/10.1007/s12206-016-1009-5>
  21. Souza CC, Arencibia RV, Costa HL, Filho AP (2005) A contribution to the measurement of circularity and cylindricity deviations. In: ABCM symposium series in Mechatronics vol 5, pp 791–800
  22. Selvarajan L, Narayanan CS, Jeyapaul R (2016) Optimization of EDM parameters on machining Si<sub>3</sub>N<sub>4</sub>-TiN composite for improving circularity, cylindricity, and perpendicularity. *Mater Manuf Process* 31(4):405–412. <https://doi.org/10.1080/10426914.2015.1058947>
  23. Dhanabalan S, Sivakumar K, Narayanan CS (2014) Analysis of form tolerances in electrical discharge machining process for inconel 718 and 625. *Mater Manuf Process* 29(3):253–259. <https://doi.org/10.1080/10426914.2013.852213>
  24. Selvarajan L, Sathiya Narayanan C, Jeyapaul R (2015) Optimization of process parameters to improve form and orientation tolerances in EDM of MoSi<sub>2</sub>-SiC composites. *Mater Manuf Process* 30(8):954–960. <https://doi.org/10.1080/10426914.2014.962041>
  25. Selvarajan L, Sathiya Narayanan C, Jeyapaul R, Manohar M (2016) Optimization of EDM process parameters in machining Si<sub>3</sub>N<sub>4</sub>-TiN conductive ceramic composites to improve form and orientation tolerances. *Meas J Int Meas Confed* 92:114–129. <https://doi.org/10.1016/j.measurement.2016.05.018>
  26. Malik A, Manna A (2018) Multi-response optimization of laser-assisted jet electrochemical machining parameters based on the grey relational analysis. *J Braz Soc Mech Sci Eng* 40(3):148. <https://doi.org/10.1007/s40430-018-1069-9>
  27. Nair A, Kumanan S (2018) Optimization of size and form characteristics using multi-objective grey analysis in abrasive water jet drilling of Inconel 617. *J Braz Soc Mech Sci Eng* 40(3):121. <https://doi.org/10.1007/s40430-018-1042-7>
  28. Suresh Kumar S, Uthayakumar M, Thirumalai Kumaran S et al (2015) Parametric optimization of wire electrical discharge machining on aluminium based composites through grey relational analysis. *J Manuf Process* 20:33–39. <https://doi.org/10.1016/j.jmapro.2015.09.011>
  29. Pandey AK, Gautam GD (2018) Grey relational analysis-based genetic algorithm optimization of electrical discharge drilling of the Nimonic-90 superalloy. *J Braz Soc Mech Sci Eng* 40(3):117. <https://doi.org/10.1007/s40430-018-1045-4>
  30. Anand G, Alagumurthi N, Elansezhian R, Palanikumar K, Venkateshwaran N (2018) Investigation of drilling parameters on hybrid polymer composites using grey relational analysis, regression, fuzzy logic, and ANN models. *J Braz Soc Mech Sci Eng* 40:214. <https://doi.org/10.1007/s40430-018-1137-1>
  31. Suresh Kumar S, Uthayakumar M, Thirumalai Kumaran S, Parameswaran P (2014) Electrical discharge machining of Al(6351)–SiC–B<sub>4</sub>C hybrid composite. *Mater Manuf Process* 29:1395–1400. <https://doi.org/10.1080/10426914.2014.952024>